View metadata, citation and similar papers at core.ac.uk
brought to you by CORE
provided by Diposit Digital de Documents de la UAB

Geologica Acta, Vol.2, Nº3, 2004, 189-201
Available online at www.geologica-acta.com
geologica acta

Tilting mechanisms in domino faults of the Sierra de San Miguelito, central Mexico

S-S. XU [1] [2] A.F. NIETO-SAMANIEGO [1] and S.A. ALANIZ-ÁLVAREZ [1]

[1] Centro de Geociencias, Universidad Nacional Autónoma de México
Apartado Postal 1-742, 76001, Querétaro, Qro., México. Nieto-Samaniego E-mail: afns@geociencias.unam.mx

[2] Instituto Mexicano del Petróleo
Eje Central Lázaro Cárdenas 152, Colonia San Bartola Atepehuácan, 07730 México, D.F., MÉXICO.
E-mail: sxu@imp.mx

ABSTRACT

A system of normal faults with similar strike that bound rotated blocks in the Sierra de San Miguelito, central Mexico, was studied to determine the genesis of rotation and to estimate the extensional strain. We show that rigid-body rotation was not the main deformation mechanism of the domino faults in this region. We propose vertical or inclined shear accommodated by slip on minor faults as the mechanism for strain in the blocks. In order to test quantitatively the amount of strain, we calculated the extension assuming vertical shear obtaining ca. e_v ~0.20. This value is in good agreement with extensions previously reported for the Mesa Central of Mexico. The bed extension required in this model reaches ca. 33% of the total horizontal extension (i. e. e_{bed} =0.34 e_v). Assuming self-similar geometry for fault displacements, it is shown that bed strain required in shear models can be liberated by the small faults. If the strain is calculated using the rigid-body rotation model, the lengthening is underestimated by up to 9%. This case study shows that shear models could be applied in volcanic zones.

KEYWORDS | Strain. Normal fault. Rigid-body rotation. Vertical shear. Mexico.

INTRODUCTION

The southern Mesa Central of Mexico was deformed by at least three major phases of Cenozoic extension. The first extensional deformation of Eocene age is recorded by the tilting of red beds that are the oldest post-orogenic sediments (Aranda-Gómez and McDowell, 1998). The second phase of extensional deformation produced numerous tectonic basins and took place in Oligocene time, between 30 and 27 Ma. The third phase of extensional deformation post-dates Miocene volcanic units and reactivated the Oligocene faults and grabens (Nieto-Samaniego et al., 1999).

The amount of Eocene extension and the direction of the principal strain axes are unknown. For the Oligocene and Miocene phases, Nieto-Samaniego et al., (1999) estimated principal horizontal extensions of 0.20 in a 259° direction and 0.11 in a 169° direction. They recognized orthorhombic fault arrays in the Mesa Central and deduced that post-Eocene strain was three-dimensional. The faults of the Sierra de San Miguelito constitute one of the

© UB-ICTJA

four sets of faults that accommodated the three-dimensional strain.

In order to improve the estimation of strain in the southern Mesa Central (Fig. 1), we measured fault displacements and the attitude of beds in a structural section presented by Labarthe-Hernández and Jiménez-López (1992) crossing the San Luis de la Paz – Salinas de Hidalgo fault system in the Sierra de San Miguelito (SSM) (Figs. 1 and 2). This fault system has been considered as "domino style" because it consists of sub-parallel faults that systematically tilt the beds to the NE (Labarthe-Hernández and Jiménez-López, 1992).

Domino faults are extensively observed in basins and other continental structures (e.g. Gibbs, 1984, 1989; McClay, 1990; Stewart and Argent, 2000). The tilting of blocks in domino faults produced by rigid-body rotation has been commonly accepted. In this model there is no internal block deformation. However, other models for explaining the tilts have been developed. For large listric faults, some authors consider that the hanging-wall block is deformed by simple shear in vertical planes assuming internal block deformation by change in bed lengths (e.g. Westaway and Kusznir, 1993). A more general shear model assumes that tilt in the hanging wall block is produced by simple shear in an arbitrary direction (White et

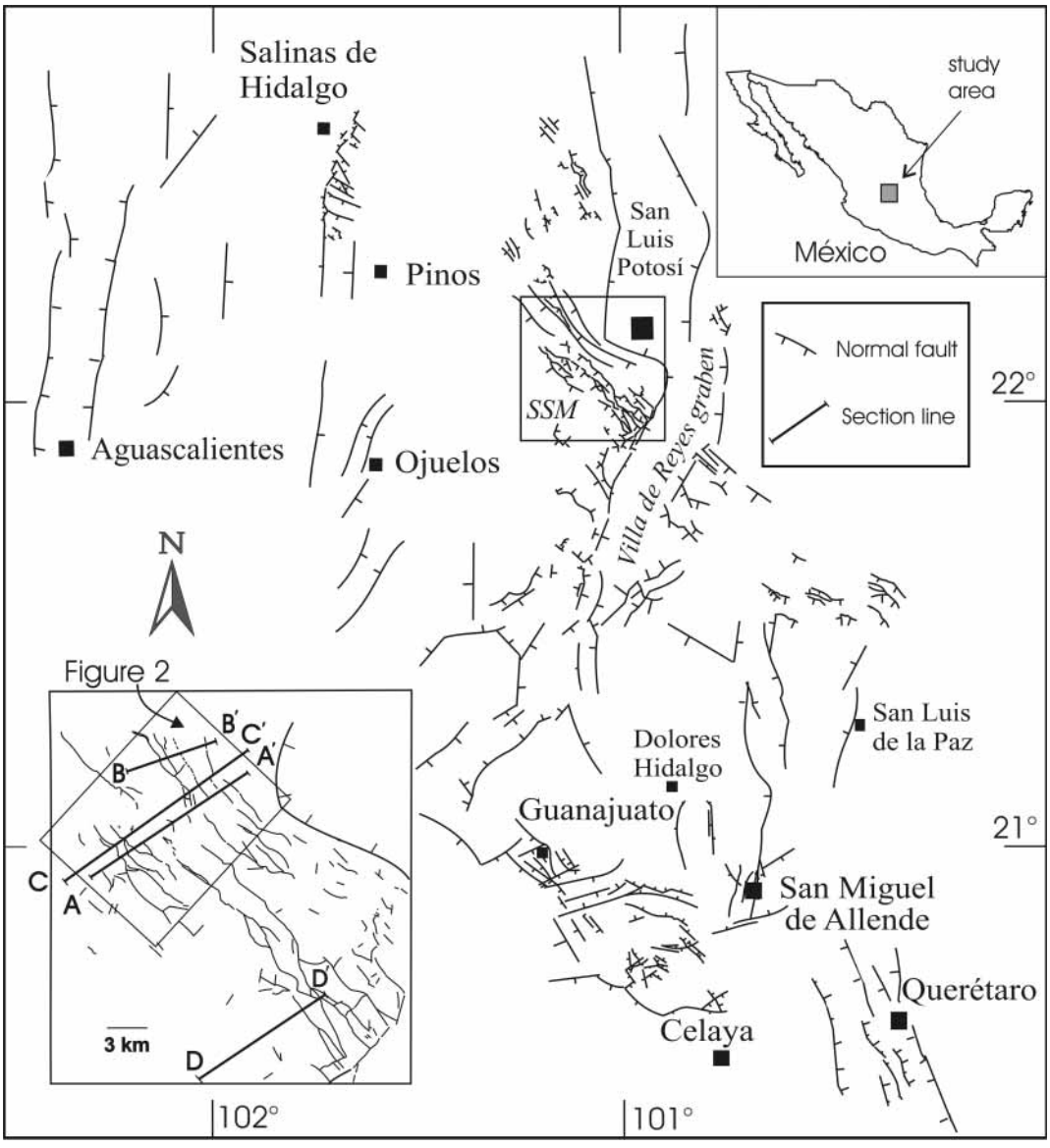

FIGURE 1 | **Map of the southern Mesa Central of Mexico showing major faults. The inset shows the faults of the Sierra de San Miguelito (SSM) and the location of structural sections.**

al., 1986; Dula, 1991). Layer-parallel shear produces internal block deformation and it can be recognized from stylolite teeth and cleavage oblique to bedding (Ferrill et al., 1998).

The main purpose of this study is determining the role of rigid body and internal deformations in the domino faults. Rigid-body rotation, vertical shear and inclined shear, require different relationships between fault and bed tilting. Those models predict different amounts of extension and initial fault dips using present dips of faults and beds. For analyzing inclined shear we need to know the fault shape in depth, which is not available in our case of study. We decided to test vertical shear and rigid body rotation models because the fault shapes at depth are not required and considered vertical shear as a special case of inclined shear. In this paper we apply strain analysis using dips of faults and beds in the volcanic region of the Sierra de San Miguelito. Also, we estimate the Cenozoic horizontal extension and document significant differences, depending on the model considered.

STRATIGRAPHY OF THE SIERRA DE SAN MIGUELITO

The stratigraphy of the southern Mesa Central was established from 1:50000 and 1:20000 scale geologic maps (Labarthe-Hernández et al., 1982; Labarthe-Hernández and Jiménez-López, 1992, 1993, 1994) and from Nieto-Samaniego et al. (1999 and references therein). The

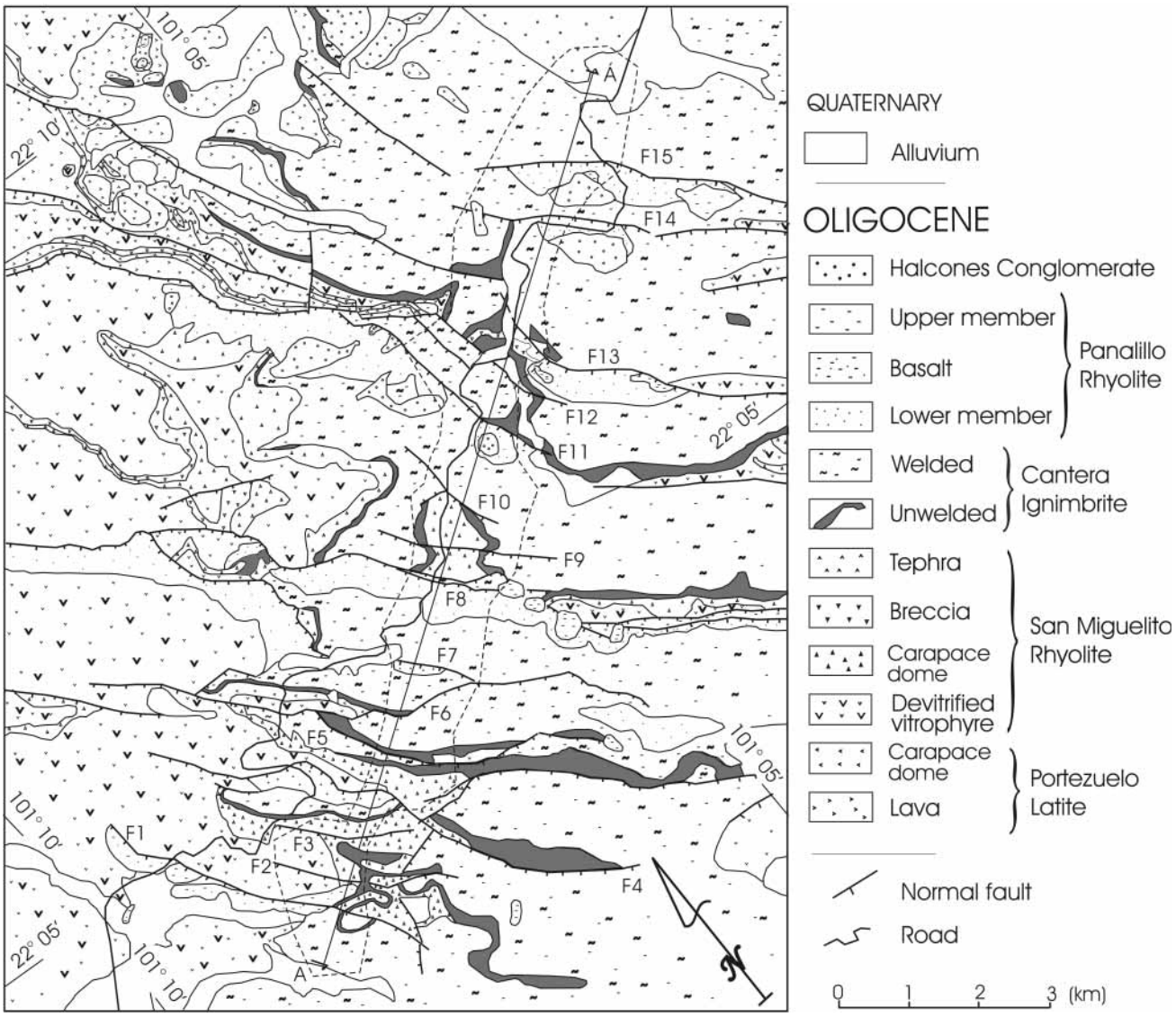

FIGURE 2 **Geological map of the Sierra de San Miguelito. Geology was modified from Labarthe-Hernández and Jiménez-López (1992). Dashed line shows the area in which bed tilts and fault dips were measured along the section A-A'.**

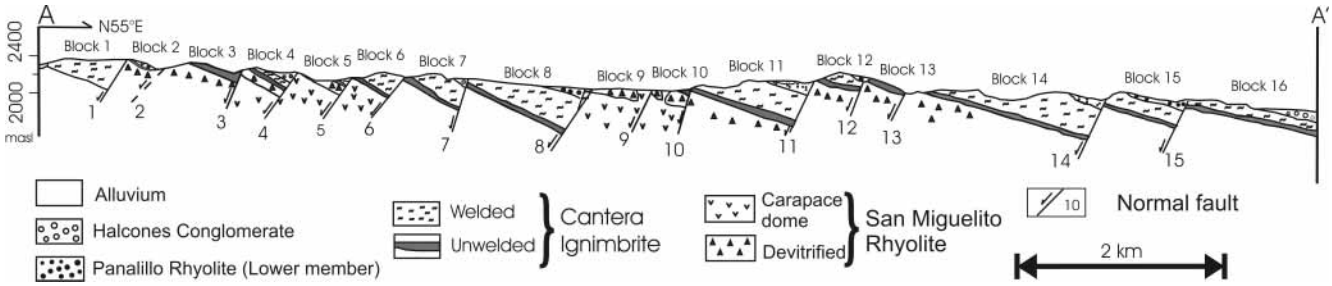

FIGURE 3 | **Cross-section A-A' in the Sierra de San Miguelito. Numbers of the faults correspond to those used in Tables 1 and 2.**

oldest unit is the Caracol Formation which is of Cretaceous age. This unit crops out only in the SE limit of the Sierra San Miguelito and consists of limestone and sandstone (Labarthe-Hernández et al., 1982). The Caracol Formation is covered by a Cenozoic acid volcanic sequence, principally Oligocene in age. In the studied area, this Oligocene stratigraphic record includes several sedimentary and volcanic units that are superficially described here:

Portezuelo Latite. This unit consists of lava flows up to 400 m thick (Labarthe-Hernández et al., 1982) that crop out, due to fault displacements, only in a few places in the central Sierra de San Miguelito.

San Miguelito Rhyolite. This unit includes a series of domes and lava flows with a thickness of up to 450 m that forms the largest volume of Cenozoic lavas in the southern Mesa Central.

Cantera Ignimbrite. This volcanic unit is made up by acid pyroclastic products that cover all the Sierra San Miguelito (Labarthe-Hernández and Jiménez-López, 1992). The lower member consists of 2-40 m of a white to pink colored unwelded ash flow, without bedding, which was deposited on a low-topographic relief. Conformably overlying the unwelded part, there is a 350 m thick, brown to gray colored, welded ignimbrite with pink tonalities. The contact between these members constitutes a good stratigraphic marker used in the construction of the structural sections (Fig. 3).

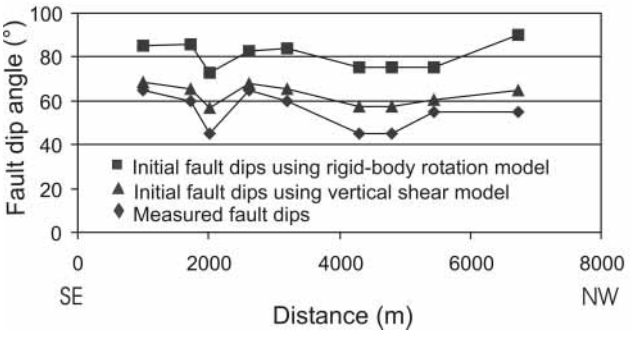

FIGURE 4| **Example of dip variation along the strike of faults in Sierra de San Miguelito. Graphs show measured dip angles and calculated initial dips for rigid body rotation and vertical shear models along the strike of Fault 4.**

Panalillo Rhyolite. This unit includes two members separated by a basaltic flow. The lower member consists of unconsolidated rhyolitic ash flow deposits and the upper one is formed by a rhyolitic welded ignimbrite. The unit covers unconformably the Cantera Ignimbrite and fills topographic depressions.

Halcones Conglomerate. This unit consists of poorly consolidated and sorted continental conglomerate with a thickness ranging from 2 to 15 m.

The above mentioned Oligocene volcanic units appear unconformably overlain by sandstone, conglomerate and fine grained deposits only within the grabens. These younger sediments are alluvial and lacustrine in origin and span in age possibly from late Oligocene to Quaternary.

GENERAL CHARACTERISTICS OF NORMAL FAULTS IN THE SIERRA SAN MIGUELITO

The studied area contains numerous normal faults with strikes of 300-340º (Fig. 2). Nearly all faults have SW dip-directions varying from 45º to 75º. The striations on fault surfaces are observed trending SW with pitch angles of 75-85º, which implies there is little displacement along the strike of the faults. These faults were classified as a domino system because they show uniform fault dip direction, uniform bedding dip direction and similar bed dip angles (Labarthe-Hernández and Jiménez-López, 1992). The faulting was dated by Nieto-Samaniego et al. (1999) to be between 30.0 to 26.8 Ma. Deformation began with the emplacement of the Cantera ignimbrite and ended with the emplacement of the upper Pananillo Rhyolite (Labarthe-Hernández and Jiménez-López, 1992). The distances between faults are not equal and fault size is variable (Figs.1, 2 and 3).

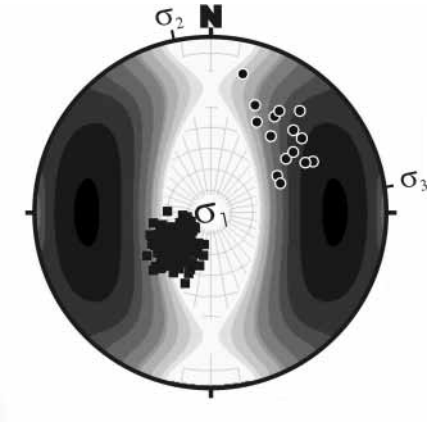

FIGURE 5 | **Equal-area net, lower hemisphere, showing in the gray zone the poles of planes that would slide before failure stress difference is reached. We use an Andersonian stress field where σ_3 is oriented 259°/00°. Orientation of σ_3 was obtained assuming that parallels the horizontal maximum extension reported by Nieto-Samaniego et al. (1999). Note that in a three-dimensional strain, maximum extension is oblique to the trend of fault striaes. This slip-rupture graph was obtained with "ReActiva" (Tolson et al., 2001), a computer program based on the Coulomb-Navier slip and rupture criteria and the general equations of Yin and Ranalli (1992). The theoretical background of this program is in Alaniz-Álvarez et al. (1998) and the program can be downloaded at: http://geologia.igeolcu.geologia.unam.mx/Tolson/SoftWare/ReActivaV24Es.exe. Different tones of gray show the potential of sliding, black being the zone of the highest potential whereas the white area indicates that rupture will be favored instead of sliding. The poles of faults (circles) are located within the darkest tones, whereas the beds (black quadrangles) have the lowest or no potential to slide. The graph shows that sliding on faults will occur prior than sliding on beds.**

There are relay structures, en échelon fault arrays, and intersections of the structures (Fig. 2), which complicate the deformation within the fault blocks. In addition, most of the faults are corrugated in the strike direction (Fig. 2), and fault dips vary along strike (Fig. 4). The differential values are larger than 10°, which is not within the range of measurement errors. Corrugations could be due to overlapping or en échelon fault arrays (Ferrill et al., 1999) and are expressed as an angular undulation (Childs et al., 1995). It is improbable that layer-parallel shear occurred in the Sierra San Miguelito because the dips of bedding are not favorable to slip (Fig. 5). Additionally, we observed rough bed contacts without slickensides and bed parallel horizontal shear bands are absent. In general, we did not observe the structures indicative of layer-parallel shear, such as those reported by Ferrill et al. (1998).

INITIAL DIPS OF NORMAL FAULTS

Under the Andersonian principle of conjugate shears, domino faults satisfy the condition

$$\cot(2\delta_0) = nC, \qquad (1)$$

where C is the coefficient of friction on the fault, δ_0 is the initial fault dip and n is +1 for reverse faults and -1 for normal faults (Westaway and Kusznir, 1993). We considered two values of C, 0.6 according to Byerlee's law and 0.8 reported by Nieto-Samaniego et al. (1997). Equation (1) shows that fault angles should be steep for the considered values of C, the expected initial dips (δ_0) are 60° and 64°.

Rigid-body rotation and vertical shear models were used to calculate the original fault dips and to determine whether our results are consistent with Andersonian theory. Table 1 shows the values of measured dips of faults (δ) and dips of beds (θ) measured near each fault in the hanging-block of the structural section A-A' (Figs. 2 and 3). We used these bed dips because they reflect the total rotation produced by the slip on the related fault.

For rigid-body rotation, tilt angles of beds and faults are equal. So, when present-day fault dips and bed tilt are given, initial fault dips (δ_r) can be obtained from

$$\delta_r = \theta + \delta. \qquad (2)$$

TABLE 1 | **Dips of faults and beds along section A-A' of Fig. 3.**

N	1	2	3	4	5	6	7	8	9	10	11	12	13	14	15
α(°)	225	245	220	239	210	250	200	215	238	226	246	220	245	230	235
θ(°)	35	25	30	12	33	26	38	23	20	17	26	15	20	15	15
δ(°)	54	45	63	54	64	45	75	55	58	75	65	67	64	65	66
δ_r(°)	89	70	117.5	88.7	122	99	143	102	99.6	107.2	113	95.1	102	98.5	93.4
δ_v(°)	64	56	69	58	70	56	78	62	63	76	69	69	68	67	68

N: progressive number assigned to measured faults; α: dip-direction of faults; θ is dip of beds near the fault in the hanging-wall; δ: the present-day dip of faults; δ_r: the initial angle of faults calculated according to the rigid-body rotation model; δ_v: the initial angle of faults calculated according to vertical shear model.

We calculated initial fault dips from the section A-A' in Fig. 3 and the result is shown in Table 1. All of the initial fault dips are steeper than the optimal values predicted by the Anderson normal faulting regime (between 60-64°), and some of them are higher than 90°.

Considering the vertical shear model of Westaway and Kusznir (1993), θ, δ, and the original fault dip (δ_v) are related by

$$\tan\delta_v = \tan\theta+\tan\delta, \quad (3)$$

We calculated δ_v values for the faults according to equation (3) (Table 1). Three initial fault dips (faults 1, 8 and 9) are in the expected range from Anderson model, but considering a compass error of ± 5° only three faults are out of range.

Table 1 shows that initial fault dips for vertical shear are more consistent with Anderson theory and initial fault dips for rigid-body rotation are more consistent with original fault dips near 90°. Considering progressive deformation, some faults could be formed later and, in our analysis they appear with very steep original dips, even greater than 90°. Faults 3, 7 and 10 in Fig. 3 could represent this case. Another explanation for the obtained steep original fault dips is that faults were originally vertical. Very steep normal faults (70-90°) have been reported in volcanic rocks such as in Yucca Mountain, Nevada (Ferrill et al., 1999) and in the Bullfrog Hills, Nevada (Maldonado, 1990). These steep faults were proposed to be the result of shear failure of rocks with relatively high friction angles, or formed by tensile failure mode (Mandl, 1988).

Faults of the Sierra de San Miguelito show better adjustment for the vertical shear model. However, it is possible that faults were formed with very steep dips and also some show a geometry suggesting that they were formed in advanced stages of progressive faulting. These uncertainties do not permit an unequivocal choice between rigid body rotation and vertical shear models from our initial fault-dip analysis.

THE CHANGE OF BED TILT ACROSS THE STRIKE OF FAULTS

One of the most evident characteristics in the area is that the dip-direction of all beds is NE. In order to determine the changes in bed tilting due to faulting across different fault blocks, we measured the structures carefully along section A-A'. This section was selected because: 1) systematic data could be obtained; 2) it crosses many faults and 3) it is nearly parallel to the average dip direction of the faults.

For the rigid-body rotation model, the bed tilt across a fault block is uniform and obeys equation (2). For the vertical simple shear model, an ideal isolated fault produces strain that changes with distance from the fault (Fig. 6A). This vertical shear is considered as distributed (Westaway and Kusznir, 1993). In the field, bed tilts would appear as in Fig. 6B, which indicates the bed tilt is larger near the fault planes. Figure 6C shows the distribution of bed tilt in a block bounded by two faults with the same displacement and attitude. The continuous line in Fig. 6C indicates the general tendency of bed tilt, and the dotted line shows the minor internal deformation that can be produced by small secondary faults or other deformation mechanisms. A more complicated case is shown in Fig. 6D, in which the distribution of bed tilt is not symmetrical when fault displacements are very different.

Bed tilt data from 16 blocks are shown in Fig. 7. Measurements for each block were made very near section A-A' and are located within the area limited by dashed line in Fig. 2. The curves in blocks 10, 11, 12, 13 and 15 show little differences among bed dips. In those cases it is not possible to conclude that bed tilts were produced by vertical shear and could be interpreted as having originated by rigid body rotation, with internal tilts produced by minor faults. In contrast, for blocks 1, 2+3, 4, 5, 6, 7, 8, 9, 14 and 16, the curves resemble Fig. 6. Tilts of beds suggest that most of the blocks could have been deformed by vertical or inclined shear. In addition, the original fault dips are in agreement with Anderson theory if vertical shear is considered. From the analysis of bed tilts and original fault dips, we interpret that vertical or inclined shear

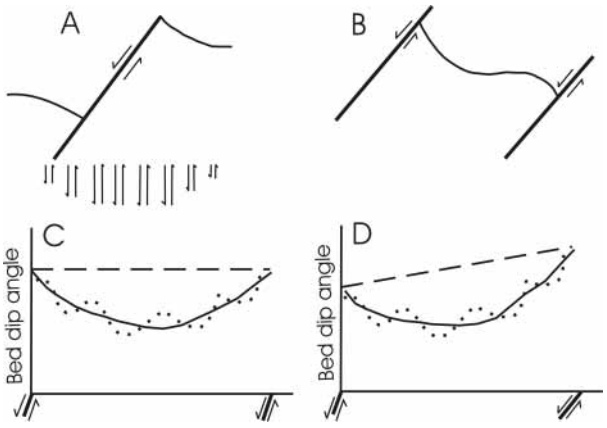

FIGURE 6 | **The distribution of shear strain and bed tilt for the vertical shear model. A) The sense and relative magnitude of vertical simple shear strain at different horizontal positions along the tilted surface and near the isolated fault plane (from Westaway and Kusznir, 1993). B) Sketch of bed tilts across a block bounded by normal faults. C) Symmetrical distribution of bed tilts. D) Asymmetrical distribution of bed tilts. Dotted lines indicate general distribution and continuous lines indicate average tendencies.**

occurred along the section. However, in many cases it is difficult to discard rigid body rotation and it is not possible to choose a unique model. More probably, different amounts of both mechanism occurred, not only along the section but also along the strike of the faults.

ESTIMATION OF EXTENSION STRAIN DUE TO NORMAL FAULTS

For vertical shear, the extension across any planar normal fault is equal to its heave. Thus, the horizontal distance between the footwall cutoff of one fault and the hanging-wall cutoff in the next fault will remain constant as deformation proceeds, maintaining its initial value (L_o in Fig. 8). So, we have DC = BC' = L_0 and the heave is h = D'B. The vertical simple shear causes the initially horizontal surface between faults to be progressively tilted by an angle q. Thus, the present length (L_b) of a bed is AC'. Using trigonometry,

$$AB = L_b \sin\theta, \text{ and} \quad (4)$$

$$L_0 = L_b \cos\theta. \quad (5)$$

Then,

$$h = D'B = AB \cot\delta = L_b \operatorname{Sin}\theta \cot\delta. \quad (6)$$

We calculated L_0 and h using L_b, θ_1, δ (measured) and equations (5) and (6) (Table 2). To estimate the extension we use, for the measured heaves, the equation $e_{vm} = (\sum h_m / \sum L_o)$ and the total extension obtained is $e_{vm} = 0.19$. For the calculated heaves, we use the equation $evc=(\sum h/\sum L_o)$ and obtained a total extension of $e_{vc} = 0.2$ (Table 2).

In addition, we compare our results with extension calculated by a rigid-body rotation mechanism. For rigid-body rotation, extension (e_r) is calculated from

$$e_r = (\sum D'C' - \sum AC')/\sum AC', \quad (7)$$

obtaining a total extension (e_r) of ca. 0.10.

In order to test the better model we compare the results with extensions obtained from the strain ellipsoid calculated by Nieto-Samaniego el al. (1999) using the model of Krantz (1988) for three-dimensional strain: [λ_1 = 1.44, oriented 259°/11°; λ_3 = 1.232, oriented 169°/02°; note that $\lambda=(1+e)^2$]. We apply the equation (Davis and Reynolds, 1996, p. 69)

$$\frac{1}{\lambda} = \frac{1}{2}\left(\frac{1}{\lambda_3} + \frac{1}{\lambda_1}\right) - \frac{1}{2}\left(\frac{1}{\lambda_3} - \frac{1}{\lambda_1}\right)\cos 2\alpha \quad (8)$$

where λ is the quadratic extension for the analyzed direction, λ_1 and λ_3 are the maximum and minimum quadratic extensions, respectively, and α the angle measured counterclockwise from λ_1 to the analyzed direction. The exten-

TABLE 2 | **Extension along the section A-A' of Fig. 3 assuming vertical shear.**

N	3	4	5	6	7	8	9	10	11	12	13	14	15
θ_1 (°)	24.5	22.7	25	28	30	24	21.6	15.25	22	13.14	18	18.5	12.4
δ (°)	63	54	64	45	75	55	58	75	65	67	64	65	66
L_b (m)	660	540	500	438	755	1120	540	400	1180	550	450	1980	790
L_0 (m)	601	498	453	387	654	1023	502	386	1094	536	428	1878	772
h_m (m)	90	180	75	195	92	360	-	28	215	45	50	180	100
h (m)	139	151	103	206	101	319	124	28	206	53	68	293	76
h/hm(%)	155	84	137	105	110	89	-	101	96	118	136	163	76
Δl (m)	59	42	47	51	101	97	38	14	86	14	22	102	18
e_{bed}	0.1	0.08	0.1	0.13	0.15	0.09	0.08	0.04	0.08	0.03	0.05	0.05	0.02
e_{hor} (for h)	0.23	0.3	0.23	0.53	0.15	0.31	0.25	0.07	0.19	0.1	0.16	0.16	0.1
e_{hor} (for h_m)	0.15	0.36	0.17	0.5	0.14	0.35	-	0.07	0.2	0.08	0.12	0.1	0.13

θ_1: Average tilt of beds in the block; L_b: present length of bed; L_0: initial length of bed; h_m: measured heave of fault.

Fault heave: $\mathbf{h=L_b\sin(\theta_1)\cot(\delta)}$
Bed stretching: $\mathbf{\Delta l=L_b-L_0}$
Bed extension: $\mathbf{e_{bed}=\Delta l/L_0}$
Horizontal value of bed extension: $\mathbf{h_{\Delta l} = (L_b - L_0)\cos(\theta_1)}$
Horizontal extension was calculated for measured and calculated heaves.
$\mathbf{e_{hor}= h/L_0}$ for calculated heave.
$\mathbf{e_{hor}= h_m/L_0}$ for measured heave.

$\mathbf{L_b}$ was measured and $\mathbf{L_0}$ estimated by $\mathbf{L_0 = L_b\cos(\theta_1)}$.
In order to calculate the total extension along sections, we used the equation $\mathbf{e_v = (\Sigma h/\Sigma Lo)}$. For fault 9, we used the value of **h** instead $\mathbf{h_m}$.
Using measured heave $\mathbf{e_{vm}}$ is **0.19**
Using calculated heave $\mathbf{e_{vc}}$ is **0.20**
Total horizontal value of bed stretching: **635** m

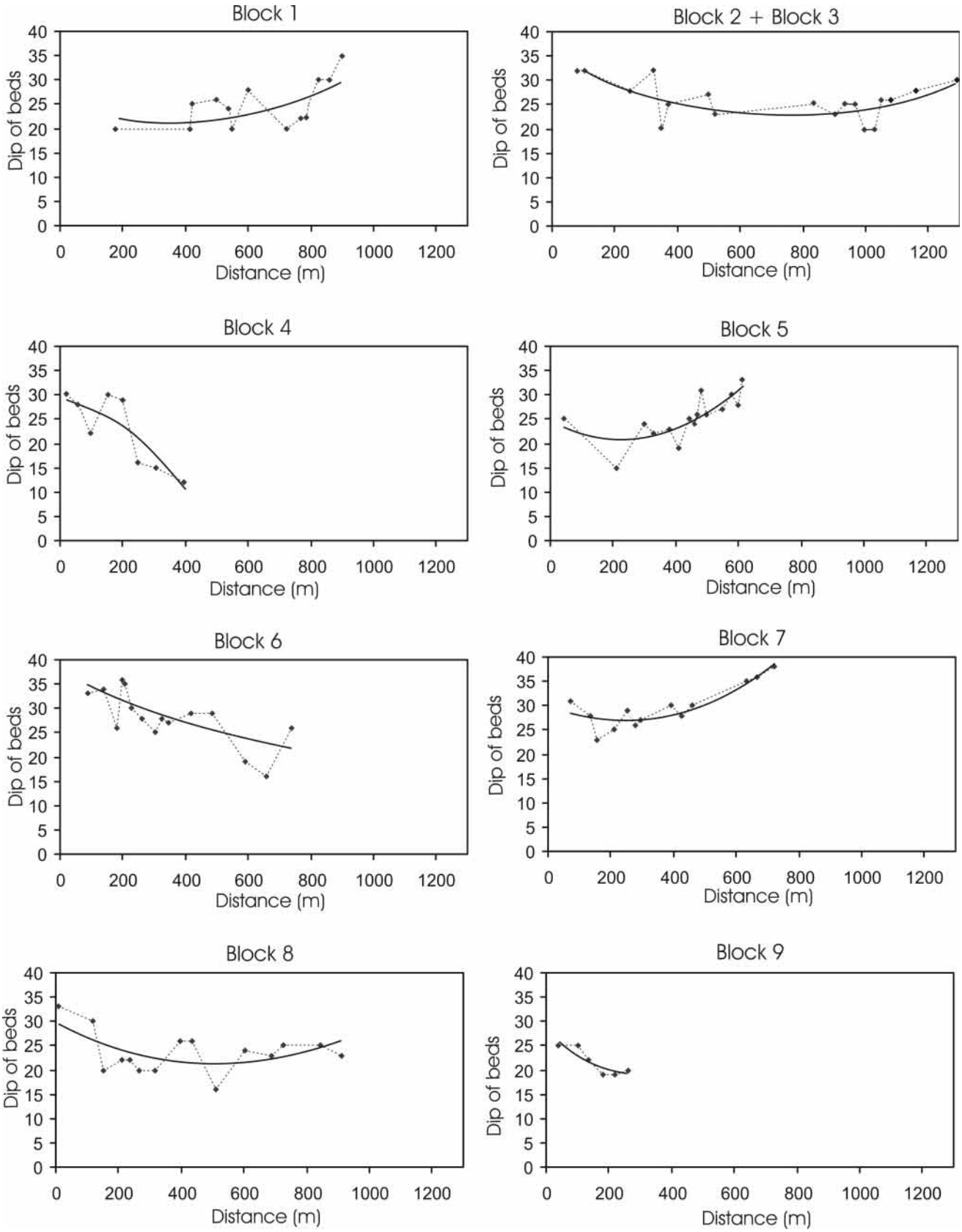

FIGURE 7 | **Distribution of bed tilts within the blocks shown in Fig. 3. Solid line indicates average tendency. Distance was measured from the southwest fault of each block.**

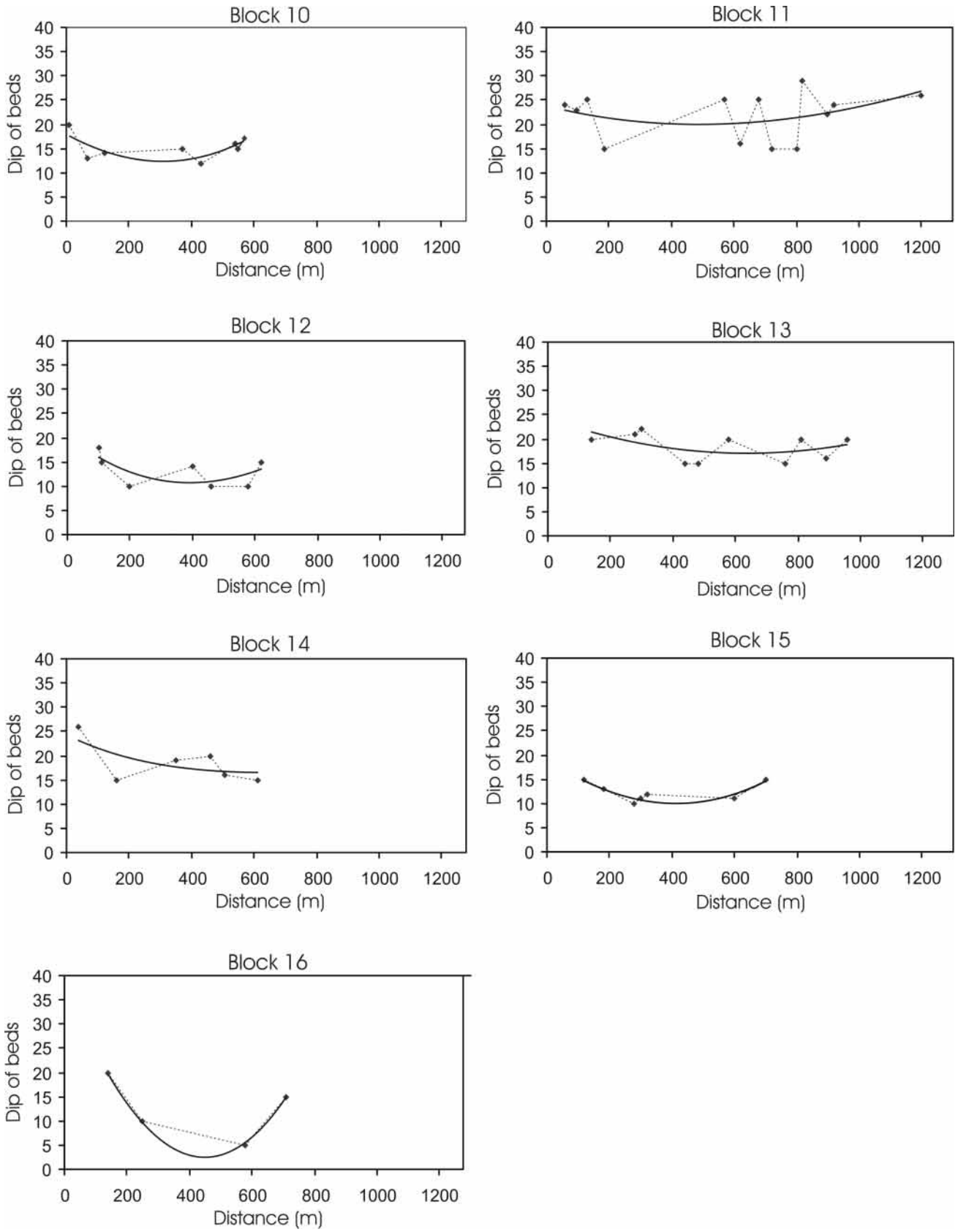

FIGURE 7 | **Continue.**

sion obtained along the studied section using the ellipsoid is $e_e = 0.18$. We see that e_v is closer to e_e than e_r. Assuming e_e as the better value of extension for the measured section, our results implies vertical (or inclined) shear as a more important mechanism of deformation than rigid-body rotation. The later underestimates extension by ca. 0.8.

There are several sources of error that produce dispersion in data and the calculated values making it impossible to obtain accurate results. Thus the obtained results are considered as an approximation, which can be used for supporting the presence or not of rigid body rotation. The main sources that we identify are:

1) The coexistence of rigid-body rotation mechanism and inclined shear. This may cause a decrease in the calculated strain. 2) Measurement error: the bedding of volcanic rocks is generally not as clear as in sedimentary rocks. This probably produces errors in field data acquisition. The measurement error for bed tilt is estimated ≤ 5º. 3) The change of bed tilt. As mentioned above, bed tilt varies largely across a block. For this reason the average bed tilts (θ_1 in Table 2) were used to calculate extension. 4) Fault corrugation: this feature would cause an error in the fault dip data because the measured points are not exactly on the points of intersection between the fault and the section. 5) Fault intersection: slip distributions near the line of intersection between two faults often show multiple slip directions (Nicol et al., 1996; Nieto-Samaniego and Alaniz-Alvarez, 1997; Maerten et al. 1999). The normal faults in San Miguelito also developed minor transverse faults that could produce oblique displacements.

THE ROLE OF SMALL FAULTS, JOINTS AND CLEAVAGES DURING VERTICAL SHEAR

Joints and cleavages

After vertical shear occurs, initial beds are tilted, thinned and lengthened (Fig. 8, Table 2). The extension of beds of individual blocks (e_{bed}) varies from 0.02 to 0.15. In fragile units near the surface, the extension is probably accomplished by minor faults distributed within the blocks. The most evident joints in ignimbrites are columnar. Two sets of joints sub-perpendicular to each other cut rocks into rhomboidal or rectangular blocks. We also observed a set of minor faults with strikes parallel to the normal faults and dips of 72-90º. The frequency is 2 minor faults for each meter along most of the cross sections. The slickensides on some minor faults and joints are observed to be nearly vertical, consistent with vertical shear. Some sub-vertical fracture cleavage zones were observed, which maintain its orientation sub-parallel to the major faults.

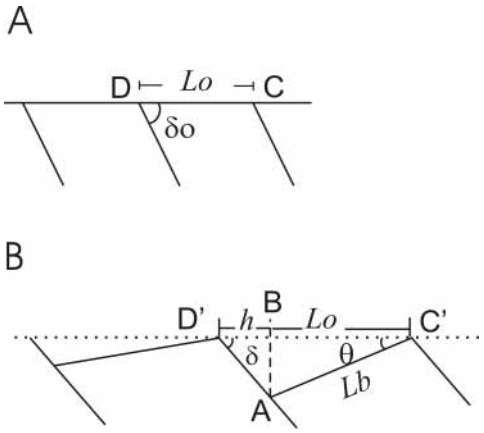

FIGURE 8 **Sketch to illustrate the relationships among parameters for a domino faults assuming vertical shear (Westaway and Kusznir, 1993).**

In the previous analysis we show that the tilting of beds were not only owing to the rigid body rotation and that vertical or inclined shear contributed to liberate deformation in the domino faults of Sierra de San Miguelito. The absence of layer parallel shear in these rocks and the presence of sub-vertical joints and minor faults suggest that they could liberate the internal extension of beds required for the vertical shear model. In order to test this idea we estimate the amount of extension due to small faults and compare it with the extension of beds obtained by applying the vertical shear model.

Finite strain due to small faults

Previous work

For many deterministic fractals, the scale invariance is obvious, but in nature self-similarity is statistical and it refers to the geometry shown by a specific parameter of the physical object. Some parameters of natural faults such as length, displacement, spacing or clustering, show a self-similar geometry (e. g., Walsh et al., 1991; Marrett and Allmendinger, 1992; Poulimenos, 2000). The self-similarity of these parameters is reflected by their power-law distributions and a plot in log-log space is commonly used to determine it.

Length (L) and displacement (D) of faults show power-law distributions and the relationship between them is crucial for strain determination because length is obtained more easily than displacement. Scholz and Cowie (1990) proposed that, if a relationship between L and D is established, the total brittle strain could be calculated when only one parameter is known.

Theoretical background

If fault displacements obey a power-law distribution, we can write

$$N = a_1 r^{-C_d}, \quad (9)$$

where N is the number of displacements larger than or equal to r; a_1 is a constant and C_d is the exponent of the cumulative displacement distribution.

The relationship between L and D has been discussed in the literature. There are two main points of view: one of them proposes that L and D are lineally related (Opheim and Gudmundsson, 1989; Scholz et al., 1993; Clark and Cox, 1996). The linear relationship has been documented analyzing a single rock type and tectonic setting (Cowie and Scholz, 1992; Dawers et al., 1993). If the relationship between displacement and length of faults is linear, the exponent of fault-length and fault-displacement cumulative distribution must be the same. Then, it is possible to calculate the finite strain by using the fault-length distribution alone.

The second point of view proposes a non-linear relationship between L and D based on a log-log graph of worldwide fault data set, including multiple lithologies and tectonic environments. There is large scatter in the *L-D* plot, and the data are enveloped by two parallel lines showing a relation of $D \propto L^{1.5}$ (Marrett and Allmendinger, 1991; Walsh et al., 1991)

Method

The displacements and fault lengths were measured on maps and sections with scales of 1:50000 and 1:20000 (Labarthe-Hernández and Jimenez-López, 1992, 1993, 1994). We calculated the relationship between fault length and displacements by selecting the points where the sections intersect the main fault and by discarding those cases where there are branches that distribute the total displacement in two or more associated faults. Multi-line data set was used for one-dimensional analysis because a single cross-section cannot provide a large enough number of faults to provide a reasonable estimation. The fault displacements were measured along four cross sections (Fig. 1). Note that the faults could be crossed in two or more points; in that case we used the displacement measured in the respective point of intersection.

Calculation of strain

We plotted lengths and displacements of faults in the graph of Fig. 9A. The graph L-D shows a large dispersion, apparently indicating a non-linear relationship for the faults of the Sierra de San Miguelito. In order to estimate the displacement distribution, we used the cumulative plots (Figs. 9B and C). Note there are both censoring (right truncation) and left truncation in Fig. 9B. The censoring has been interpreted as an underestimation of the large-scale values (Jackson and Sanderson, 1992; Pickering et al., 1995). The left truncation indicates incomplete sampling in our studied area (e.g. Pickering et al., 1995). After eliminating left truncation we obtained an exponent value of 0.63. Plotting the data of each section separately, this method was proposed by Yielding et al. (1996), we obtained an envelope slope of 0.66. Although the availa-

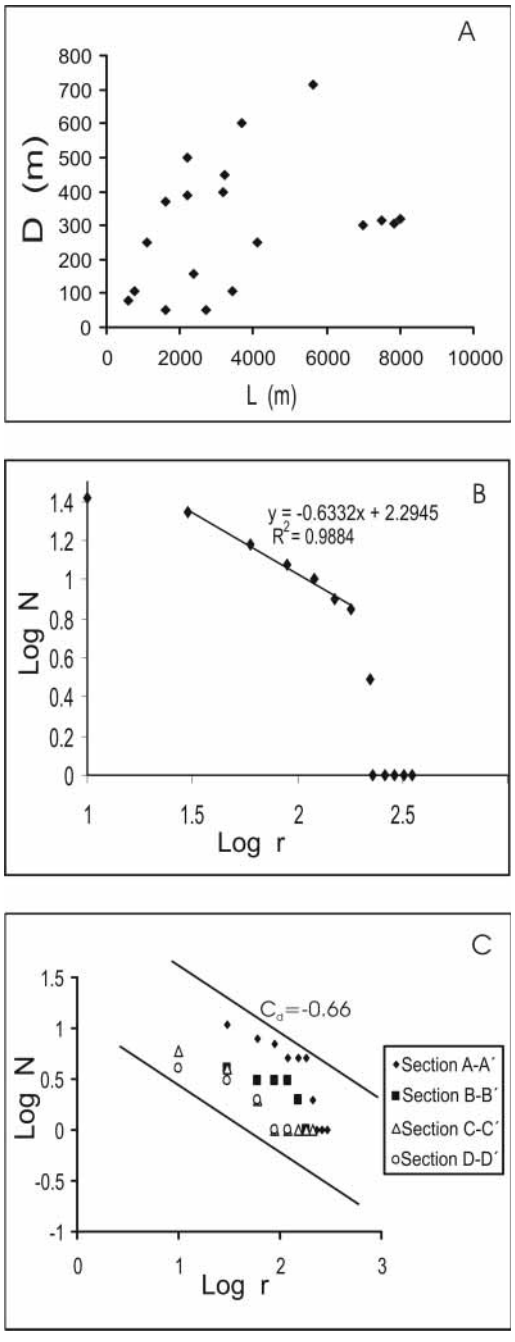

FIGURE 9 | **The graphs were constructed using data obtained from sections indicated in Fig. 1. A) Length - Displacement plot, note that there is no a clear tendency. B) Log-Log diagram of cumulative number versus displacement *(r)* using all data. C) Log-Log diagram of cumulative number versus displacement *(r)* of each section separately.**

ble data used to calculate the power law distribution of fault displacements could be considered poor, the little difference between exponent values obtained by these two methods give some confidence in the C_d value.

From Marrett and Allmendinger (1990), the sum of heaves for small faults can be estimated by

$$h_s = h_n \frac{C_d}{1-C_d}(N+1)\left(\frac{N}{N+1}\right)^{\frac{1}{C_d}} \quad (10)$$

where h_s is the sum of the heaves for the small faults, h_n is the smallest heave of the large faults and N is the number of faults observed in one-dimensional sampling. We calculated h_s using $C_d = 0.63$, $h_n = 28$ (see Table 2) and obtained $h_s = 601.42$ m. This result is near to the value obtained for the heaves due to bed stretching calculated from the vertical shear model ($\sum h_{\Delta L} = 635$ m, see Table 2), suggesting that tilt and lengthening of beds really result from displacements on small faults. If $C_d = 0.66$ is used, $h_s = 680.12$ and this value is larger than the heaves due to bed stretching. These results show that displacement of small faults can accommodate the horizontal strain required by the vertical shear model. From Table 2, we obtain $\sum L_0 = 9211$ m, and using the cumulative curve of Fig. 9B, which produce a more accurate exponent, the extension due to small faults is $e_s = h_s/\sum L_0 = 0.065$ which is ca. 33% of the total extension.

CONCLUSIONS

The calculated initial fault dips are not consistent with the angles predicted by Anderson theory, opening up two possibilities: 1) deformation took place by vertical or inclined shear, or 2) faults formed with original dip angles near 90°. The initial dip angle analysis does not permit an unequivocal choice between those possibilities.

The dip of beds shows that tilts were larger near the faults bounding blocks. It is impossible to produce this tilt pattern by rigid body rotation. We interpret that internal block deformation is the main evidence of vertical or inclined shear.

Vertical shear produces greater extension than rigid-body rotation. We calculated the extensions along one section obtaining $e_{vc} = 0.20$ for vertical shear and ca. $e_r = 0.10$ for rigid-body rotation. The value of extension for vertical shear is in good agreement with the previous estimation (e_e=0.18) for the Mesa Central reported by Nieto-Samaniego et al. (1997, 1999). The rigid-body rotation model underestimates the lengthening by up to 8%.

Although we do not have a good data base, a power-law distribution of fault displacements in the Sierra San Miguelito is supported by the available information. The stretching of beds required by the vertical shear model could be produced by small faults, and probably joints played an important role during vertical shear. The calculated extension due to small faults (e_s =0.065) is ca. 33% of the total extension considering large and small faults.

Generalizing, our data show that vertical or inclined shear took place in meso- or even small-scale faults in the volcanic rocks of Sierra de San Miguelito, and the model of Westaway and Kusznir (1993) can be applied in order to calculate extensions. The bed strain required by vertical shear probably was accommodated by displacement along small faults or joints in shallow crustal levels.

ACKNOWLEDGEMENTS

Thanks to R. Westaway for explaining to us the method of extensional calculation for vertical shear. We wish to thank D. J. Sanderson, Alan Morris, David Ferrill and Barbara Martiny for their pertinent suggestions in an earlier version of the manuscript. Comments of F. Sàbat and an anonymous reviewer are acknowledged. This work was supported by projects PAPIIT-IN113399 and CONACYT-33087-T.

REFERENCES

Alaniz-Álvarez, S.A., Nieto-Samananiego, A.F., Tolson, G., 1998. A graphical technique to predict slip along a preexisting plane of weakness. Engineering Geology, 49, 53-60.

Aranda-Gómez, J.J., McDowell, F.W., 1998. Paleogene extension in the Southern Basin and Range Province of Mexico: Syndepositional tilting of Eocene red beds and Oligocene volcanic rocks in the Guanajuato mining district. International Geology Review, 40, 116-134.

Childs, C., Watterson, J., Walsh, J.J., 1995. Fault overlap zones within developing normal fault systems. Journal of Geological Society of London, 152, 535-549.

Clark, R.M., Cox, S.J.D., 1996. A modern regression approach to determining fault displacement-length scaling relationships. Journal of Structural Geology, 18, 147-152.

Cowie, P.A., Scholz, C. H., 1992. Displacement-length scaling relationship for faults: data synthesis and discussion. Journal of Structural Geology, 14, 1149-1156.

Davis, G., Reynolds, S.J., 1996. Structural geology of rocks and regions. New York, ed. John Wiley and Sons Inc., second Edition, 779 pp.

Dawers, N.H., Anders, M.H., Scholz, C.H., 1993. Growth of normal faults: Displacement-length scaling. Geology, 21, 1107-1110.

Dula, W.F. Jr., 1991, Geometric models of listric normal faults and rollover folds. American Association of Petroleum Geologists Bulletin, 75, 1609-1625.

Ferrill, D.A., Morris, A.P., Jones, S.M. Stamatakos, J.A., 1998. Extensional layer-parallel shear and normal faulting. Journal of Structural Geology, 20, 355-362.

Ferrill, D.A., Stamatakos, J.A., Sims, D., 1999. Normal fault corrugation: implications for growth and seismicity of active normal faults. Journal of Structural Geology, 21, 1027-1038.

Gibbs, A.D., 1984. Structural evolution of extensional basin margins. Journal of the Geological Society, 141, 609-620.

Gibbs, A.D. 1989. Structural style in basin formation. In: Tankard, A.J. Balkwill, H.R. (eds.). Extensional tectonics and stratigraphy of the north Atlantic Margins. Memoir American Association of Petroleum Geologists, 46, 81-93.

Jackson, P., Sanderson, D.J., 1992. Scaling of fault displacements from the Badajoz-Cordoba shear zone, SW Spain. Tectonophysics, 210, 179-190.

Krantz, R.W., 1988, Multiple fault sets and three-dimensional strain: theory and application: Journal of Structural Geology, 10, 225-237.

Labarthe-Hernández, G., Jiménez-López, L.S., 1992. Características físicas y estructura de lavas e ignimbritas riolíticas en la Sierra de San Miguelito S. L. P. Universidad Autónoma de San Luis Potosí, Instituto Geología, Folleto técnico (Open File Report) No. 114, 31 pp.

Labarthe-Hernández, G., Jiménez-López, L.S., 1993. Geología del domo Cerro Grande, Sierra de San Miguelito S. L. P. Universidad Autónoma de San Luis Potosí, Instituto Geología, Folleto técnico (Open File Report) No. 117, 22 pp.

Labarthe-Hernández, G., Jiménez-López, L.S., 1994. Geología de la porción sureste de la Sierra de San Miguelito S. L. P. Universidad Autónoma de San Luis Potosí, Instituto Geología, Folleto técnico (Open File Report) No. 120, 34 pp.

Labarthe-Hernández, G., Tristán-González, M., Aranda-Gómez, J.J., 1982. Revisión estratigráfica del Cenozoico de la parte central del Estado de San Luis Potosí. Universidad Autónoma de San Luis Potosí, Instituto de Geología, Folleto Técnico (Open File Report) No. 85, 208 pp.

Maerten, L., Willemse, E.J.M., Pollard, D.D., Rawnsley, K., 1999. Slip distributions on intersectioning normal faults. Journal of Structural Geology, 21, 259-271.

Maldonado, F. 1990. Structural geology of the upper plate of the Bullfrog Hills detachment fault system, southern Nevada. Geological Society of America Bulletin, 102, 992-1006.

Mandl, G., 1988. Mechanics of tectonic faulting. New York, ed. Elsevier, 408 pp.

Marrett, R., Allmendinger, R.W., 1990. Kinematic analysis of fault-slip data. Journal of Structural Geology, 12, 973-986.

Marrett, R., Allmendinger, R.W., 1991. Estimates of strain due to brittle faulting: sampling of fault populations. Journal of Structural Geology, 13, 735-738.

Marrett, R., Allmendinger, R.W., 1992. Amount of extension on "small" faults: An example from the Viking Graben. Geology, 20, 47-50.

McClay, K.R., 1990. Extensional fault systems in sedimentary basins: a review of analogue model studies. Marine and Petroleum Geology, 7, 206-233.

Nicol, A., Walsh, J.J., Watterson, J., Bretan, P.G., 1996. Three dimensional geometry and growth of conjugate normal faults. Journal of Structural Geology, 17, 847-862.

Nieto-Samaniego, A.F., Alaniz-Álvarez, S.A., 1997. Origin and tectonic interpretation of multiple fault patterns. Tectonophysics, 270, 197-206.

Nieto-Samaniego, A.F., Alaniz-Álvarez, S.A., Labarthe-Hernández, G., 1997. La deformación cenozoica poslaramídica en la parte meridional de la Mesa Central, México. Revista Mexicana de Ciencias Geológicas, 14, 13-25.

Nieto-Samaniego, A.F., Ferrari, L., Alaniz-Álvarez, S.A., Labarthe-Hernández, G., Rosas-Elguera, J., 1999. Variation of Cenozoic extension and volcanism across the southern Sierra Madre Occidental Volcanic Province, México. Geological Society of America Bulletin, 111, 347-363.

Opheim, J.A., Gudmundsson, A., 1989. Formation and geometry of fractures and related volcanism of the Krafla fissure swarm, northeast Iceland. Geological Society of America Bulletin, 101, 1608-1622.

Pickering, G., Bull, J.M., Sanderson, D.J., 1995. Sampling power-law distributions. Tectonophysics, 248, 1-20.

Poulimenos, G., 2000. Scaling properties of normal fault populations in the western Corinth graben, Greece: implications for fault growth in large strain setting. Journal of Structural Geology, 22, 307-322.

Scholz, C.H., Cowie, P.A., 1990. Determination of geologic strain from faulting using slip measurement. Nature, 346, 837-839.

Scholz, C.H., Dawers, N.H., Yu, J-Z., Anders, M.H., 1993. Fault growth and fault scaling laws: Preliminary results. Journal of Geophysical Research, 98, 21951-21962.

Stewart, S.A., Argent, J.D., 2000. Relationship between polarity of extensional fault arrays and presence of detachments. Journal of Structural Geology, 22, 693-711.

Tolson, G., Alaniz-Álvarez, S.A., Nieto-Samaniego, 2001. ReActiva, a plotting program to calculate the potential of reactivation of preexisting planes of weakness. Instituto de Geología, Universidad Nacional Autónoma de México, http://geologia.igeolcu.unam.mx/Tolson/SoftWare/ReActivaV24En.exe.

Walsh, J., Watterson, J., Yielding, G., 1991. The importance of small-scale faulting in regional extension. Nature, 351, 391-393.

Westaway, R., Kusznir, N., 1993. Fault and bed "rotation" during continental extension: block rotation or vertical shear? Journal of Structural Geology, 15, 753-770.

White, N.J., Jackson, J.A., Mckenzie, D.P., 1986. The relationship between the geometry of normal faults and that of the sedimentary layers in their hanging walls. Journal of Structural Geology, 8, 879-909.

Yielding, G., Needham, T., Jones, H., 1996. Sampling of fault populations using sub-surface data: a review. Journal of Structural Geology, 18, 135-146.

Yin, Z.M., Ranalli, G., 1992. Critical stress difference, fault orientation and slip direction in anisotropic rocks under non-Andersonian stress systems. Journal of Structural Geology, 14, 237-244.

Manuscript received March 2003;
revision accepted October 2003.